3106–3118 *Nucleic Acids Research, 2010, Vol. 38, No. 9* *Published online 19 January 2010*
doi:10.1093/nar/gkp1216

Structural and mechanistic insights into *Helicobacter pylori* NikR activation

C. Bahlawane[1], C. Dian[2], C. Muller[3], A. Round[4], C. Fauquant[1], K. Schauer[3], H. de Reuse[3], L. Terradot[2,*] and I. Michaud-Soret[1,*]

[1]CNRS UMR 5249 Laboratoire de Chimie et Biologie des Métaux; Commissariat à l'Energie Atomique (CEA), Direction des Sciences du Vivant (DSV), Institut de Recherches en Technologies et Sciences pour le Vivant (iRTSV); Université Joseph Fourier, 17 avenue des Martyrs, Grenoble F-38054 cedex 9, [2]The European Synchrotron Radiation Facility, BP 220 F-38043 Grenoble cedex 9, [3]Unité de Pathogenèse de *Helicobacter*, Département de Microbiologie, Institut Pasteur, 28 rue Docteur Roux, 75724 Paris Cedex 15 and [4]European Molecular Biology Laboratory, Grenoble Outstation, 38042 Grenoble Cedex 9, France

Received October 15, 2009; Revised December 16, 2009; Accepted December 17, 2009

ABSTRACT

NikR is a transcriptional metalloregulator central in the mandatory response to acidity of *Helicobacter pylori* that controls the expression of numerous genes by binding to specific promoter regions. NikR/DNA interactions were proposed to rely on protein activation by Ni(II) binding to high-affinity (HA) and possibly secondary external (X) sites. We describe a biochemical characterization of HpNikR mutants that shows that the HA sites are essential but not sufficient for DNA binding, while the secondary external (X) sites and residues from the HpNikR dimer–dimer interface are important for DNA binding. We show that a second metal is necessary for HpNikR/DNA binding, but only to some promoters. Small-angle X-ray scattering shows that HpNikR adopts a defined conformation in solution, resembling the *cis*-conformation and suggests that nickel does not trigger large conformational changes in HpNikR. The crystal structures of selected mutants identify the effects of each mutation on HpNikR structure. This study unravels key structural features from which we derive a model for HpNikR activation where: (i) HA sites and an hydrogen bond network are required for DNA binding and (ii) metallation of a unique secondary external site (X) modulates HpNikR DNA binding to low-affinity promoters by disruption of a salt bridge.

INTRODUCTION

As essential metal ions can also be toxic when present in excess, cells have developed strategies to control their intracellular concentration (1). Metal homeostasis is finely tuned by metal transporters, metal storage proteins and metalloregulatory proteins. Many metalloregulators are transcription factors that bind metal cations to regulate gene expression by specific DNA interaction. In the case of nickel, NikR proteins are the major actors in the regulation of nickel homeostasis in bacteria (ref. 2 and refs. therein). In *Escherichia coli*, NikR (EcNikR) binds nickel and recognizes a specific operator sequence located upstream of the *nikABC* operon coding for the nickel ABC transporter system and represses its transcription (3). In the human pathogen *Helicobacter pylori*, NikR (HpNikR) plays a critical role (4) since *H. pylori* survival relies on the production of active urease and hydrogenase, enzymes that require nickel for their catalytic activities (5,6). HpNikR is pleiotropic and controls the expression (activation or repression) of a large set of genes involved not only in nickel and iron homeostasis but also in acid stress response (7–9); however, no consensus sequence for the operator could be clearly identified (10–13). HpNikR-dependent direct regulation has been shown for seven genes/operons: *ureA* (urease), *frpB4* and *nixA*

*To whom correspondence should be addressed. Tel: +33 4 38 78 99 40; Fax: +33 4 38 78 54 87; Email: imichaud@cea.fr
Correspondence may also be addressed to Laurent Terradot. Tel: +33 4 76 20 94 54; Fax: +33 4 76 20 94 00; Email: terradot@esrf.fr
Present addresses: K. Schauer. Molecular Mechanisms of Intracellular Transport, UMR 144 CNRS, Institut Curie.12, rue Lhomond, 75005 Paris, France.
C. Fauquant. Laboratoire d'Enzymologie et Biochimie Structurales UPR3082 CNRS, Gif-sur-Yvette, France. Bât 34 ,Rue de la terrasse, 91198 Gif sur Yvette, France.

The authors wish it to be known that, in their opinion, the first two authors should be regarded as joint First Authors.

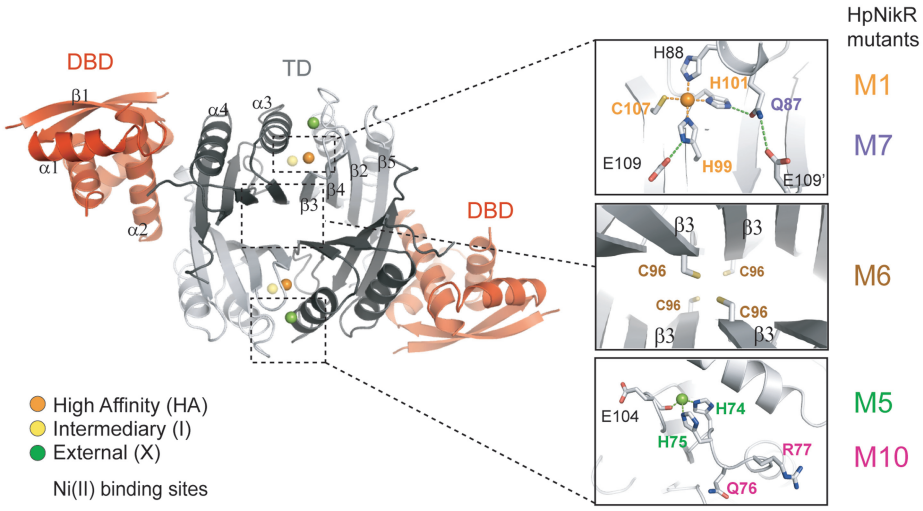

Figure 1. Structural organization of Nickel bound HpNikR. **(Left)** Ribbon diagram of the overall Ni-HpNikR structure (14) in a view parallel to the crystallographic 2-fold axis. The tetramerization domain (TD) is coloured in black (chains A and C) and grey (chains B and D) and DNA-binding domains (DBD) in red. Nickel ions bound to high affinity (HA), intermediary (I) and external (X) sites are represented as spheres coloured in orange, yellow and green, respectively. **(Right)** Detailed view of the Ni(II)-binding sites HA and X and of the TD interface. Side chains of residues involved are represented in ball and stick. The residues mutated are indicated in the colour corresponding to the mutant: M1 (H99A, H101A, C107A), orange; M5 (H74G, H75G), green; M6 (C96S) brown; M7 (Q87F), violet and M10 (Q76A, R77A), pink. This colour-coding will be used in all the figures unless specified.

(nickel transporter), *fecA3* (metal transporter), *exbB* (energy machinery for metal uptake), *nikR* and *fur* (metalloregulators).

Structural studies have shown that NikRs are tetrameric with two main domains; a tetramerization domain (TD) flanked by two dimeric ribbon–helix–helix DNA-binding domains (DBDs) (14–16) (Figure 1). NikRs were observed in different conformations: an open conformation (15,16) in which the DBDs are linearly placed on each side of the TD and a closed *trans*-conformation where the DBDs are placed on opposite sides of the TD (14,16). However, the conformation suited for NikR proteins to bind their operator was established by the crystal structure of EcNikR/DNA complex (17) to be a closed *cis*-conformation where the two DBDs are located on the same side of the EcNikR TD and are bound to the two halves of the operator sequence (17).

NikR's activation depends on the incorporation of nickel ions at specific binding sites (18,19). NikRs bind Ni(II) to four high-affinity (HA) sites located at the TD interface. The architecture of the HA sites is conserved among NikRs. There, nickel ions are coordinated in a square planar geometry by a cysteine and two histidines from one subunit and one histidine from the adjacent subunit [(14) and Figure 1]. When HA sites are occupied, a conserved network of hydrogen bonds is formed at the TD interface that connects nickel ions two by two. Secondary nickel-binding sites have been described in NikR proteins but appear more species-specific (14,16,17,20–23).

Secondary low-affinity (LA) sites, positioned at the interface between the TD and DBDs, were identified in EcNikR and in *Pyrococcus horikoshii* NikR (PhNikR) (16,17). However, these sites were occupied by potassium ions in the EcNikR/DNA complex and by nickel ions in the Ni-PhNikR crystal structure (16,17). Several studies have suggested that metal binding to these LA sites could improve EcNikR affinity for its target DNA (24–27). To fulfil its regulatory function, EcNikRs was proposed to be in an equilibrium state between open and closed conformations in the apo-form. Nickel binding to HA sites would induce a significant shift of the two dimers, stabilize the TD interface and position EcNikR onto the DNA helix via short-range allosteric effects (16,25). The binding of nickel ions to LA sites would then lock NikR in the closed *cis*-conformation necessary for the interaction with DNA and repression function.

To what extent this model is conserved for HpNikR is unknown. For instance, the residues forming LA sites are conserved, but no metal ions were observed there in the structures of Ni–HpNikR (14) and DNA-binding properties of LA-mutated HpNikR were not affected (28). Instead, another secondary nickel-binding site was identified at the surface of the tetramerization interface in the structure of nickel-bound HpNikR and named external site (X) (Figure 1). The X site is absent in Ni-EcNikR structures, which raises questions about its conservation in NikRs and its relevance to HpNikR function (17). Another nickel-binding site was detected in Ni-HpNikR, but considered as an intermediary site (I), on the road of nickel incorporation to the HA sites, involving residues from both the X and HA sites [Figure 1; (14)]. Finally, the nature of the metal bound to these secondary sites and their role(s) in HpNikR function are still unclear. As a matter of fact, it was proposed that HpNikR can be activated by nickel only (13,29,30) but other studies suggested that other metal ions were required (19).

To gain insights into the molecular mechanism of HpNikR activation, we have investigated the structural

and molecular properties of HpNikR and HpNikR mutants by using Ultraviolet–visible (UV/vis) spectroscopy, electrophoretic mobility shift assay (EMSA), small-angle X-ray scattering (SAXS), X-ray crystallography and *in vivo* mutagenesis of *H. pylori*. Our results shed light on key molecular details of the effects of nickel on HpNikR activity, insights from which we derive a model for HpNikR activation, also consistent with the existing literature. This model involves a first activation step where occupancy of the HA site establishes a hydrogen bond network required for DNA binding. In a second step, HpNikR/DNA interaction is tuned by the secondary external (X) site in response to nickel and, possibly, other metal ions. These mechanisms might explain the unique properties of HpNikR and provide the protein with different regulatory features associated with its various functions in the bacterium.

MATERIALS AND METHODS

Chemicals

All regular chemicals were purchased from Sigma–Aldrich.

Strains and plasmids

Strains and plasmids used in this study are listed in the Supplementary Table S1.

Plasmids engineering

For mutants M1, M5, M6 and M7, the mutated full-length *nikR* sequences were polymerase chain reaction (PCR)-amplified from the previously constructed pILL2224 derivative plasmids (14), containing the different *nikR* mutations introduced by QuickChange mutagenesis. The PCR products, amplified with primers N7 (cgggatccATCAAAACTCCCTCCATAGAGCGC) and N9 (ggaattccatATGGATACACCCAATAAAGAC GATTCAATC), were inserted into the pET11 expression vector. The mutant M10 was constructed by GeneSOEing (31) using N9 and N10rev (TAA TTC **CGC TGC** GTG GTG ATC ATA AAT CAC) on the one hand, and N7 and N10fwd (GAG GAG **GGA GGG** GAA TTA AAG GAG GGG ATG) on the other hand, using pET11aNikR as template. Subsequently, the two PCR products were used as template for the fusion PCR with N7 and N9 as primers. After NdeI–BamHI digestion, the final product was introduced in the pET11a and checked by sequencing.

Helicobacter pylori growth

Helicobacter pylori strains used for western blotting were cultivated in Brucella liquid medium supplemented with 0.2% β-cyclodextrine (Sigma) and with an antibiotic and fungicide cocktail consisting of vancomycine ($5\,mg\,l^{-1}$), polymyxine B ($2500\,U\,l^{-1}$), trimethoprim ($5\,mg\,l^{-1}$) and amphotericine B ($4\,mg\,l^{-1}$). Flasks were incubated at 37°C under microaerophilic conditions. Kanamycin ($20\,\mu g\,ml^{-1}$) for *nikR* null mutant and chloramphenicol ($20\,\mu g\,ml^{-1}$) for the other *nikR* mutants were added to the growth medium. When indicated, the cultures were supplemented with 5 or 10 μM $NiCl_2$.

Protein over-expression and purification

HpNikR and mutated proteins were expressed in *E. coli* BL21 DE3 and purified by a combination of anion exchange and gel-filtration chromatographies, as reported elsewhere (14,32). The concentrated proteins were stored at –80°C in 10% glycerol and 0.1 mM dithiothreitol (DTT). After purification, nickel content was estimated to be very small (concentration <5% of the protein subunit concentration) and the buffer was systematically exchanged using micro-bio spin 6 column prior use. No significant difference was noted in the protein yield or gel-filtration profiles between the mutated and the wild-type proteins.

Crystallization of NikR mutants and data collection

Crystallization experiments of NikR mutants were set up at room temperature using the hanging-drop vapour-diffusion method by mixing a protein solution at $10\,mg\,ml^{-1}$ in 20 mM Tris–HCl (pH 7.5), 150 mM NaCl with an equal volume of reservoir solution. M1 crystals were grown under similar crystallization conditions as those described for wild-type NikR with a reservoir solution of 0.6 M Na formate and 100 mM (Na) citrate pH 4.0. Cryoprotection of M1 crystals was achieved as reported for the crystals of the wild-type protein (14). M5, M6 and M7 crystals were obtained in different crystallization conditions, consisting of 0.4–0.7 M ammonium sulphate and 100 mM (Na) citrate pH 5–5.4. Native M5, M6 and M7 crystals were cryo-protected by soaking crystals in a cryosolution containing 0.4 M ammonium sulphate, 50 mM (Na) citrate pH 5.2–5.4, 1 M Na formate and 25% glycerol and then flash-frozen in liquid nitrogen. Ni-M5 data set was obtained by soaking apo-M5 crystals three days in the same cryosolution supplemented with 100 mM $NiSO_4$. Data were collected at 100 K at the ESRF beamlines. Diffraction images from NikR mutant crystals were integrated, scaled and merged with X-ray Detector Software (33). Data set statistics were obtained from SCALA. The intensities were converted to structure factors using the program TRUNCATE. Similarly to the wild-type protein, M1 and M5 crystals belong to $P6_122$ space group with one dimer per asymmetric unit (AU), M7 crystals belong to the space group $P4_32_12$ containing two molecules in the asymmetric unit. M6 crystals were found to have a $P2_12_12_1$ space group consisting of one biological tetramer per asymmetric unit.

Structure determination and refinement

Apo-NikR mutant structures were determined by molecular replacement (MR) using wild-type apo-HpNikR structure (pdb code 2ca9) as a template. MR calculations were performed using either MOLREP or PHASER programs (34). Mutant structures were refined against data using PHENIX.REFINE (35), alternated with model building with COOT (36). Restrained refinement was carried out in combination with translation/

libration/screw (TLS)-motion refinement using two TLS groups for M1, M5 and M7 (group 1 consists of residues 7–63 from chains A and B; group 2 consists of residues 64–148 from chains A and B), while four TLS groups were used for M6 instead of two. Ni-bound M5 crystal structure was also solved by MR using apo-M5 crystal structure as a template for the search. Summary of the composition and geometry of the final models along with relevant refinement statistics are presented in Supplementary Table S2. The programs MOSFLM, MOLREP, SCALA and TRUNCATE are part of the CCP4 software package (37). Figures were generated with Pymol software (DeLano scientific LLC, San Carlos, CA, USA, http://www.pymol.org). The coordinates of HpNikR mutants structures have been deposited in the PDB (entry codes M1: 2wvb, M5: 2wvc, M6: 2wvd, M7: 2wve, NiM5: 2wvf).

Nickel binding to HpNikR and derivatives followed by UV/vis spectroscopy

UV-vis spectra were collected at 25°C on U-300 spectrophotometer (Hitachi) equipped with a temperature controller. Concentrated $NiSO_4$ was progressively added to 100 µl HpNikR at 200 µM in 20 mM HEPES at pH 7.5 with a final volume change <4% in a 1-cm path-length quartz cuvette. All experiments were performed at least in triplicate with two different protein batches. Spectra were recorded between 280 and 750 nm and the extinction coefficients at 305 nm of Ni(II)-HpNikR and Ni(II)-mutants were determined by plotting the absorbance difference between the apo and holo proteins at 305 nm versus metal concentration and fitting the data up to 1 metal equivalent to a straight line. Kinetics of Ni(II) binding were investigated by acquiring a spectrum every minute during 40 min. Nickel dissociation was monitored by adding ethylenediaminetetraacetic acid (EDTA; 10 mM final) to a 1:1 Ni–protein complex and recording spectra continuously for 1 h.

EMSA conditions

The two strands of a 32-bp DNA fragment of the *nixA* promoter region (–15 to +21 relative to the transcription starting site) were purchased from Sigma Genosys. One strand was labelled with γ-^{32}P-ATP by incubation with the T4 polynucleotide kinase (Fermentas) at 37°C for 30 min. Non-incorporated nucleotides were removed with a micro-bio spin 6 column (Biorad). Oligonucleotides were then annealed by incubation of the mixture at 85°C for 15 min and slowly cooled down.

Radio-labelled DNA (450 pM) was incubated for 30 min with HpNikR or mutant proteins at room temperature in 15 µl binding buffer (20 mM Bis–Tris Borate pH 7.4, 50 mM KCl, 100 µM $NiSO_4$, 3 mM $MgCl_2$, 2.5% glycerol, 0.1% Triton X-100 and 1.5 µg ml^{-1} dI–dC). 6% native polyacrylamide gels (29:1) containing 100 mM Bis–Tris borate buffer at pH 7.4 and 100 µM $MnCl_2$ (prepared in the same running buffer) were pre-run for 30 min at 150 V before loading the samples and running the gels also at 150 V. DNA binding was also observed with $NiCl_2$ instead of $MnCl_2$ in the running buffer; however, some smears were observed, probably resulting from complex dissociation during electrophoresis. Radio-labelled bands were detected on a storage phosphor screen for at least 2 h and visualized using a Cyclone Imager (PerkinElmer). Intensities of the free and protein-bound DNA were analysed to estimate the dissociation constant (K_d) of each mutated protein for the *nixA* duplex by plotting the ratio free DNA/retarded DNA as a function of the protein concentration.

Western blots

Proteins from *H. pylori* were extracted using the Bugbuster Protein extraction reagent according to the manufacturer's instructions (Novagen). Protein concentrations were measured with Bradford assay (BioRad). Ten micrograms of crude extracts were separated by 12.5% sodium dodecyl sulphate-polyacrylamide gel electrophoresis (SDS-PAGE) and blotted on a polyvinylidene fluoride (PVDF) membrane (Millipore). Correct calibration of the samples was verified by Coomassie staining of gels loaded with the same amounts of total proteins (Supplementary Figure S3). NikR and UreA were detected with rabbit polyclonal antibody raised against NikR (7) and UreA (38) from *H. pylori*. Binding of the ECL anti-rabbit immunoglobulin G (IgG) antibody, coupled to peroxidase produced in horse (GE Healthcare), was revealed with the ECL Plus reagent (Pierce).

SAXS

Data were collected at the BioSAXS station (ID14EH3) at the ESRF, (http://www.esrf.fr/UsersAndScience/Experiments/MX/About_our_beamlines/ID14-3). ID14-3 is a fixed energy (13.32 keV, $\lambda = 0.931$ Å) station optimized for solution scattering from biological macromolecules. Samples were exposed using 30 µl of protein solution (in 50 mM HEPES pH 7.5) loaded into a 2-mm quartz capillary mounted in vacuum using an automated robotic system, which enables the sample to pass through the beam during exposure to minimize the effect of radiation damage. Two-dimensional (2D) scattering images were collected using the Vantec2000 gas-filled detector from Bruker at a distance of 1.745 m from the sample. Standard data collection time of 5 min was used for all samples, split into 10 individual 30-s frames. Individual time frames were processed automatically and independently by the data collection software (BsxCUBE) developed at the ESRF, yielding individual radially averaged curves of normalized intensity versus scattering angle ($s = 4\pi\mathrm{Sin}\theta/\lambda$). Time frames are combined excluding any data points affected by aggregation induced by radiation damage to give the average scattering curve for each measurement. The scattering from the buffer alone was measured before and after each sample measurement and the average of the scattering before and after each sample is used for background subtraction using the program PRIMUS (39) from the ATSAS package developed by EMBL Hamburg. HpNikR and M7 mutant were analysed in the presence and in the absence

of 1 equivalent Ni(II) per subunit. Nickel-metalled samples were prepared using the same protocol as described previously with the only difference of the addition of $NiCl_2$. Ni-bound samples were also verified for their DNA-binding activity before and after measurements. A range of protein concentrations obtained by dilution (1.5, 7.5 and 15 mg ml^{-1}) were measured in order to assess and remove any concentration-dependent inter-particle effects, none was observed. Scattering data were collected for each sample in 10 individual 30-s frames in order to assess any changes due to radiation-induced aggregation, none was observed for any samples. As no radiation-induced aggregation effects were observed, the high concentration data were used (exhibiting the best signal-to-noise ratio) to find the model-independent scattering parameters R_g, estimated Mw (Guinner analysis), volume (Porod) and Dmax (GNOM) using Primus as well as for further analysis.

HpNikR experimental curve was used to identify the conformation of the protein in solution, by comparing it with theoretical scattering curves of three different conformations of HpNikR: open, closed-*trans* and closed-*cis*. To generate the HpNikR model in open conformation, HpNikR structure was first superimposed to PhNikR (pdb 2bj3) based on the TD only. The DBDs were then manually positioned using the orientation and positioning of α2 helices from apo-PhNikR as a template. Loops α2–β2 were finally reconstructed. Analysis of the TD/DBD interface was done and no clash could be observed. HpNikR model in a *cis*-conformation was built by superimposing the TD apo-HpNikR chain A to HpNikR chain B generating a modified dimer A/B. The modified A/B dimer was added to the unmodified dimer C/D reconstructing a full-*cis* model. The theoretical scattering curves from the different NikR models were compared to the merged scattering curve using the program CRYSOL (40).

RESULTS

HpNikR mutants targeting residues from HA (M1, triple mutant H99A, H101A, C107S) and external X (M5, double mutant H74G, H75G) sites, and a residue participating in the hydrogen bond network between HA sites (M7 single mutant Q87F) were previously shown to disrupt the nickel response when introduced in *H. pylori* cells (14). M1 and M7 mutants presented a severe sensitivity to nickel, similar to a *ΔnikR* while M5 displayed an intermediate phenotype, such as M6 (C96S), a mutant targeting the TD interface (see Figure 1). Here, we present a biochemical and structural characterization of purified M1, M5, M6 and M7 mutant proteins. An additional M10 (Q76A, R77A) mutant was constructed to identify the role of these residues, proposed to be involved in DNA binding in EcNikR (17). The positioning of these mutations is shown on the Figure 1. The resulting HpNikR mutant proteins were purified using the same procedure as the wild type, leading to analogous yield and homogeneity.

Ni(II) binding to HpNikR and HpNikR mutants

The ability of the purified HpNikR mutated proteins to bind Ni(II) at the final HA sites was measured by UV/vis spectroscopy at 305 nm corresponding to a Cys 107 $S^{\gamma} \rightarrow$ Ni ligand to metal charge transfer (LMCT) band (18,32). The difference between the absorption spectra of the apo and holo proteins upon Ni(II) addition shows the appearance of peaks at 305 and 475 nm (Supplementary Figure S1A), except for mutant M1. The binding profiles of HpNikRs are shown in Figure 2A by the changes in absorbance at 305 nm upon the addition of up to 3 equivalents of $NiSO_4$ per subunit. The intensity at 305 nm increased linearly up to one equivalent nickel per monomer similarly for HpNikR, M5, M6, M7 and M10 mutants and saturation was observed at a stoichiometry of 1 Ni(II) per monomer. This indicated that HpNikR mutants accommodate one nickel per monomer i.e. four HA sites per HpNikR tetramer.

It is noteworthy that a difference in the kinetics of Ni(II) binding was observed between M6 and the other proteins. Ni(II) binding to M6 required more than 20 min to reach equilibrium, while the reaction took between 3 and 8 min for HpNikR, M5, M7 or M10 (Supplementary Figure

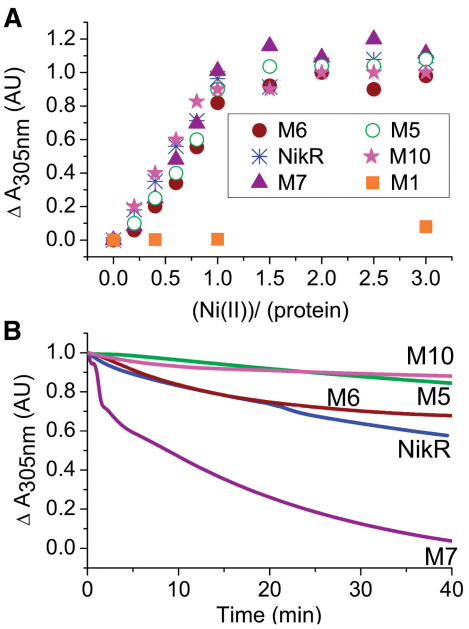

Figure 2. Ni(II) binding to NikR and M5, M6, M7 and M10 derivatives and kinetics of metal release for HpNikR and derivatives. **(A)** Comparison of the binding profiles of HpNikR, M5, M6, M7 and M10 determined by the changes in absorbance at 305 nm upon the addition of up to 3 equivalents of $NiSO_4$. The presented data correspond to the difference in the absorption at 305 nm between the absorption spectra of the holo and apo forms for each protein. Data were collected at the equilibrium, 30 min after addition of $NiSO_4$ to 200 μM of protein solution in HEPES 20 mM, pH 7.4. The results are homogenous (variation is <5%) and were reproduced at least three times with two different protein batches. **(B)** Comparison of the kinetics of Ni(II) release from HpNikR, M5, M6, M7 and M10. UV-visible absorption spectra were continuously measured for 1 h after EDTA addition. The changes in absorbance at 305 nm are presented as function of time after addition of 10 mM EDTA to a Ni(II)–protein complex with a 1:1 stoichiometry. Experiments were reproduced three times giving similar results.

S1B). The kinetics of Ni(II) release from the HA sites has also been investigated by adding a chelating agent in excess, EDTA, to 1:1 Ni–protein complexes (Figure 2B). HpNikR and M6 showed similar release rates of nickel ions and small differences were observed between HpNikR and mutants M5 and M10. A more significant difference was found with M7, which showed an accelerated Ni(II) release (Figure 2B).

Thus, the Ni(II) binding study demonstrates that HpNikR mutations affecting the X site, I site and residues proposed to bind DNA backbone (M10) do not affect nickel incorporation at HA sites contrarily to residue affecting directly the HA site (M1). However, the residue Q87 appears important to stabilize Ni(II) at HA sites, and mutating C96 into a serine reduces Ni(II) incorporation rate.

In vitro DNA-binding properties

The DNA-binding properties of the HpNikR mutants were investigated by using two approaches. First, we used EMSA with a 32-bp DNA duplex, which was successfully used to demonstrate the direct regulation of *nixA* expression by HpNikR (8,11). A 327-bp PCR fragment, corresponding to a DNA region within the *fur* gene, was used as negative control. The *nixA* duplex was retarded by the addition of increasing HpNikR, M6, M5, M10 protein concentrations (Figure 3A). The ratios between retarded and free DNA, obtained from three independent experiments, were plotted as a function of the protein concentration (Figure 3B). It resulted in a K_d for *nixA* of 1.3 nM for HpNikR, 1.6 nM for M6, 18 nM for M5 and ~100 nM for M10. These values are slightly smaller than those recently described for HpNikR (11), possibly due to experimental differences in the purification process and/or the method used to determinate the K_d. These results indicate a lower affinity of M5 and M10 for the *nixA* promoter region (~13 versus 80 times lower) compared with wild-type HpNikR. No dissociation constant could be determined for M7 and M1, since these proteins were found unable to retard efficiently the migration of the duplex, even at high protein concentrations.

A second approach was used to compare the DNA-binding properties of the proteins by implementing a nuclease protection assay in solution (Supplementary Data). Briefly, in this assay, the *exbB–nikR* intergenic region was cloned in a pHP2G plasmid and a SspI site was inserted within the spacer of the HpNikR box found upstream of *exbB* (41). As a result, the binding of HpNikR to its target on the plasmid should protect against the SspI endonuclease. The results obtained are consistent with the EMSA study, and indicate that HpNikR and M6 can protect DNA from SspI digestion and therefore binds efficiently to the *exbB–nikR* region (Supplementary Figure S2). In contrast, the endonuclease profiles indicate that M5 binds weakly, while M1 and M7 did not bind to the target DNA.

The DNA-binding studies show that mutating Q87 considerably reduces HpNikR DNA-binding activity. Moreover, H74 and H75 (belonging to the X site) and Q76 and R77, corresponding to a loop interacting with DNA in EcNikR/DNA complex (19), seem to be important for DNA-binding efficiency.

Metal requirement for DNA binding

The metal requirements for HpNikR activation are still under debate. Some groups proposed complete protein activation *in vitro* with nickel only (13,29,30), while others suggested that secondary metal ions were required (19). To better understand the role of secondary metal ions, we performed EMSA using two different conditions: in the presence of Ni(II) (Figure 4A) and in the presence of Ni(II) and Mn(II) (Figure 4B). Three different promoter regions were used: p_{ureA}, considered as a 'HA' promoter, and two 'LA' promoters, p_{nikR} and p_{exbB}, as classified by Dosanjh *et al.* (11). The results indicate that NikR is able to efficiently retard the migration of p_{ureA} both in Ni(II) and Ni(II)/Mn(II) conditions. In the case of p_{nikR} or p_{exbB}, HpNikR binding was detected in the Ni(II)/Mn(II) conditions but not in the Ni(II) conditions. This suggests that

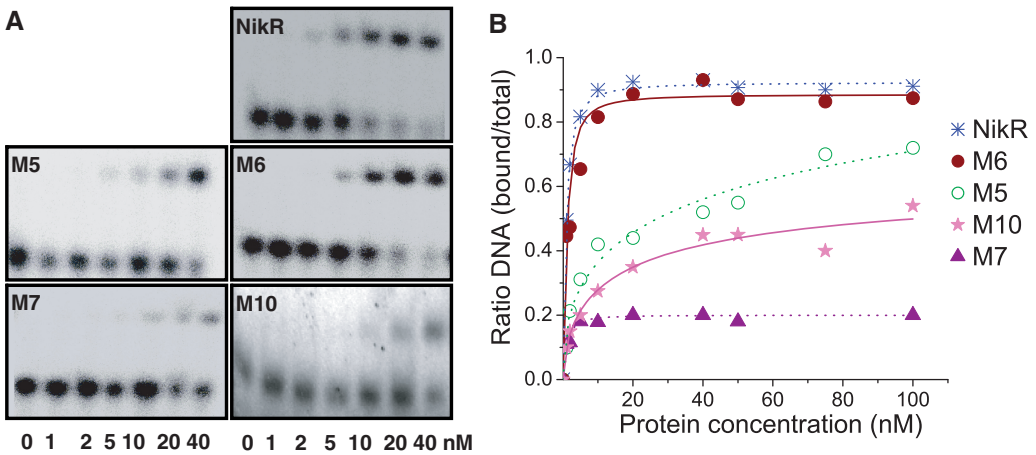

Figure 3. DNA-binding properties of HpNikR and derivatives to P*nixA*. **(A)** Titration of the *nixA* affinity of HpNikR and mutants by EMSA with increasing protein concentrations from 1 to 40 nM against 450 pM P_{nixA}. Binding buffer contained 100 µM $NiSO_4$ while gel and running buffers contained 100 µM $MnSO_4$. **(B)** Binding curves corresponding to the average fraction of bound P_{nixA} related to the total labelled DNA were fitted using the Hill equation with an *n*-value of 1.5. Each plot is the average of four data sets. Variations were <5%.

other metals are required for efficient DNA binding but only for a category of the HpNikR promoter regions.

Impact of NikR mutations on the *in vivo* response to nickel of the *ureA* and *nikR* genes

We then examined the response of two *H. pylori* genes known to be directly regulated by HpNikR, positively for *ureA* and negatively through auto-regulation for *nikR*, in strains carrying a *nikR* gene with the M5 or the M6 mutations. The amounts of UreA and HpNikR in wild-type 26695 strain, the isogenic mutants *ΔnikR*, M5 and M6 grown with 5, 10 µM $NiCl_2$ or without added nickel were examined by western blotting using specific antibodies. In the wild-type strain, the amounts of UreA protein gradually increased upon nickel addition, whereas HpNikR amount decreased (Figure 5). As expected, this regulation was lost in the *ΔnikR* mutant. In the M6 mutant, the C96S mutation did not significantly affect the response of the expression of the two proteins to nickel. In contrast, in the M5 mutant, the expression of UreA and HpNikR was not modified with increasing nickel concentrations, indicating that M5 lost its activity *in vivo*. This suggests that residues belonging to the X site are important for the regulation of *ureA* and *nikR* gene expression *in vivo*.

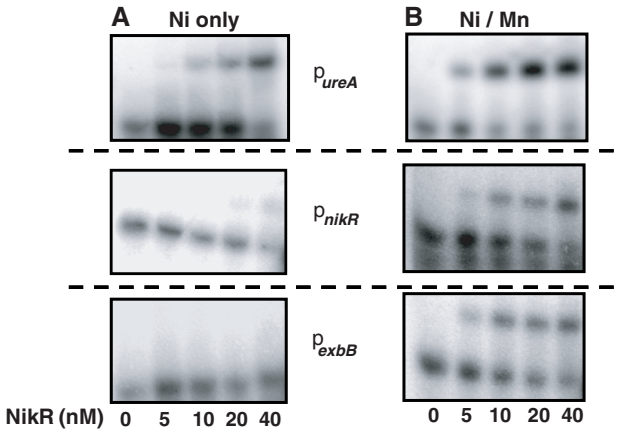

Figure 4. DNA-binding properties of HpNikR to P*nixA*, P*ureA* and P*exbB* in Ni-only and Ni/Mn conditions. The condition described in **(A)** corresponds to the one described by Zambelli *et al.* (13) with binding reactions performed in HEPES binding buffer [20 mM HEPES pH 7.85, 50 mM KCl, 0.01% Triton X-100, 0.1 mM DTT, 10% glycerol (v/v), 6 µg ml^{-1} sonicated sperm DNA, 100 µM $NiSO_4$]. After a 15 min incubation with increasing HpNikR concentrations, complexes were separated on 5% acrylamide/bisacrylamide (19:1) gels, in MOPS/NaOAc running buffer (20 mM MOPS, 5 mM NaOAc pH 7.0), run at room temperature for 110 min at 170 V. EMSA conditions in **(B)** were Bis–Tris buffer and the binding conditions described in 'Materials and Methods' section of the manuscript (binding buffer with $NiSO_4$ and running buffer with $MnSO_4$).

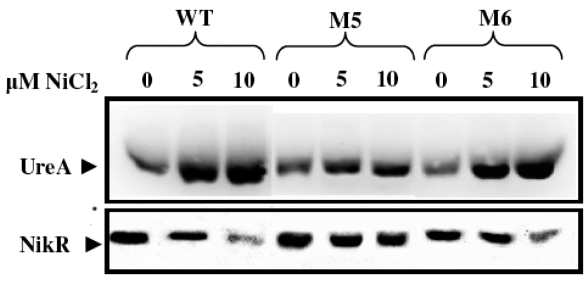

Figure 5. Western blots of total lysates of *H. pylori* WT 26695, M5 and M6 in response to increasing $NiCl_2$ concentrations. Ten micrograms of total proteins were extracted from cultures grown to the mid-log phase in the absence or presence of $NiCl_2$ and loaded on polyacrylamide gels, transferred to nitrocellulose membranes and revealed with antibodies directed against UreA and NikR. Coomassie-stained gels were used as loading control and are presented in Supplementary Figure S3.

SAXS study of HpNikR

To determine whether nickel binding to HA sites induces conformational changes of the DBDs of HpNikR in solution, we performed SAXS measurement of apo-HpNikR and Ni-HpNikR. Experimental scattering curves are shown in Figure 6A and global shape parameters derived are presented in Table 1. The scattering patterns of apo- and Ni-HpNikR were very similar, indicating that Ni-activation of HpNikR did not generate large conformational changes. Only a small difference

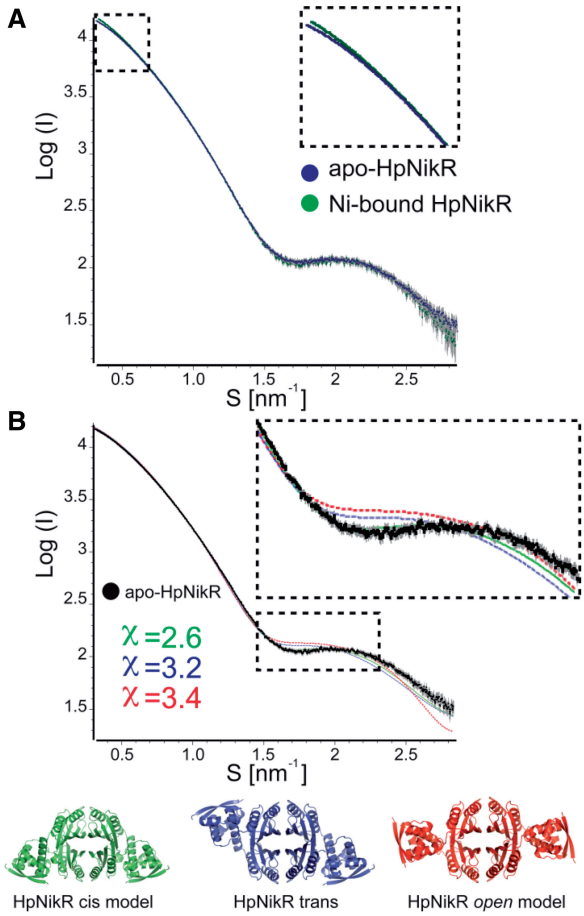

Figure 6. Small-angle X-ray diffraction (SAXS) of both apo and Ni-bound HpNikR. **(A)** Experimental scattering profiles from the apo (blue circles) and holo (green circles) HpNikR showing that both curves are almost equivalent. Dashed line square shows a close-up of the low-angle region of both experimental curves. **(B)** Experimental scattering profile from the apo-HpNikR (black spheres) compared with the theoretical curves calculated for HpNikR in closed *cis*- (green), closed *trans*- (blue) and open (red) conformations. The best fit is obtained with the closed *cis*-conformation as shown by the chi between experimental and theoretical curves obtained using Crysol.

Table 1. Global shape parameters derived from SAXS of apo and Ni(II)-bound HpNikR and M7 mutant

	R_{gc} (nm)	D_{max} (nm)	Estimated Mw (KDa)	Porod volume (nm^3)
apo-HpNikR	2.822	10	62	113
Ni-bound HpNikR	2.927	10	67	120
apo-M7	2.976	10	65	120
Ni-bound M7	2.976	10	65	120

The radius of gyration of the cross section (R_{gc}), the excluded volume of the particle in solution (Porod volume) and the maximum dimension (D_{max}) calculated from the scattering data are presented.

in the low-angle region could be noticed, where the Ni-HpNikR scattering profile displays a higher I(0) value than apo-HpNikR (Figure 6A). Since no radiation damage was observed on the collected frames and Ni-HpNikR was stable in solution, a higher flexibility of Ni-HpNikR could explain a larger Ni-bound form.

To identify the conformation of HpNikR in solution, the scattering profiles measured from apo- and Ni-HpNikR were compared against those calculated from HpNikR models using CRYSOL (40). Scattering curves of HpNikR crystal structure (*trans*-conformation) and two theoretical HpNikR models in *open*- and *cis*-conformation were used ('Material and methods' section). The best fit was obtained with the *cis*-HpNikR model (chi value of 2.6), in good agreement with the scattering pattern of HpNikR as seen in Figure 6B. In contrast, the calculated patterns for the open or *trans*-conformations (as seen in HpNikR crystal structure) did not fit as well (chi values of 3.2 and 3.4). In addition, we analysed M7 mutant in the presence and the absence of Ni(II). As shown in Supplementary Figure S6, M7 and Ni-M7 scattering curves are equivalent to the HpNikR and Ni-HpNikR ones, respectively, suggesting that M7 and HpNikR have very similar conformations in solution. These results show that HpNikR adopts a conformation that resembles more the *cis*-conformation in solution and that nickel binding at the HA sites does not generate large conformational changes of HpNikR DBDs.

In the crystal structure of HpNikR, the protein adopts a *trans*-conformation, which contrasts with its state in solution. No *cis*-conformation structure has been obtained for NikR proteins in the absence of DNA, suggesting that the *cis*-conformation of NikRs might not be able to sustain molecular contacts encountered in crystals in the absence of nickel and DNA. More importantly, *trans*- and *cis*-conformations NikRs have a closed conformation, where the DBDs are packed against the TD. No difference could be observed between the TD interface of holo- and DNA-bound EcNikR (17) suggesting that the molecular contacts of the nickel-binding sites and between the TDs and DBDs are equivalent in *cis*- and *trans*-conformation.

Apo and Ni-bound structures of HpNikR mutants

The effects of the mutations on HpNikR were therefore examined by determining the structures of HpNikR variants M1, M5, M6 and M7 in apo and Ni-bound

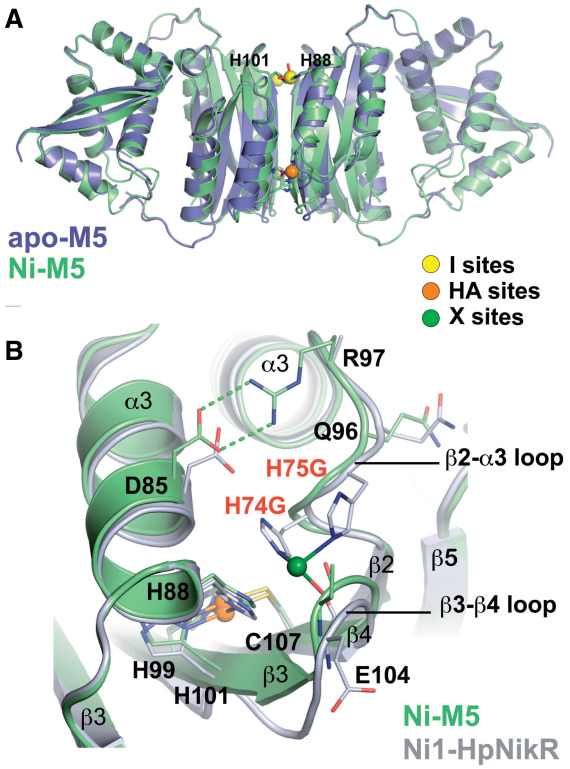

Figure 7. Apo- and Ni-bound structures of M5 reveal an absence of X sites. **(A)** Structural comparison of apo-M5 (blue) with Ni-M5 structure (green). **(B)** Detailed comparison of Ni-M5 structure (green) with Ni1-HpNikR (grey). Ni-M5 structure was superimposed onto Ni1-HpNikR [r.m.s deviation of 0.98 Å (531 Cα)]. Nickel ions bound to HA, I and X sites are indicated as sphere and coloured as in Figure 1. Amino acids involved in nickel binding are shown as balls and stick and coloured by atom type (carbon as the ribbon, green; oxygen, red; nitrogen, blue; and sulphur, orange). Nickel coordination and hydrogen bonds are presented as full lines and green broken lines, respectively. Residues from M5 mutant are labelled in red.

forms (Supplementary Table S2). All mutants showed a secondary structure topology almost identical to HpNikR and displayed the *trans*-conformation. The HA-deleted mutant, M1 (H99A, H101A, C107S), adopts also a closed *trans*-conformation (Supplementary Figure S4). Moreover, no significant changes are observed at the TD interface compared to HpNikR. This suggests that the organization of the TD interface is independent of the residues that bind nickel at the HA site.

The structure of M5 (H74G, H75G) was determined at 2.1 Å (Figure 7 and Supplementary Table S2). The residues H74 and H75 were previously identified in the Ni1-HpNikR structure (pdb code 2cad) as being involved in both the intermediary I (H74) and external X (H74, H75) sites. The structure of apo-M5 is almost identical to HpNikR apart from the mutated residues. Apo-M5 crystals were then soaked in a cryoprotectant containing 100 mM $NiSO_4$ for 3 days resulting in Ni-M5 crystal structure (Figure 7A, Supplementary Table S2). Ni-M5 structure is almost identical to the Ni1-HpNikR structure (14) with four nickel-bound per tetramer, two at HA sites and two to modified I sites. The modified I site of Ni-M5 structure has a low occupancy (0.3) and presents

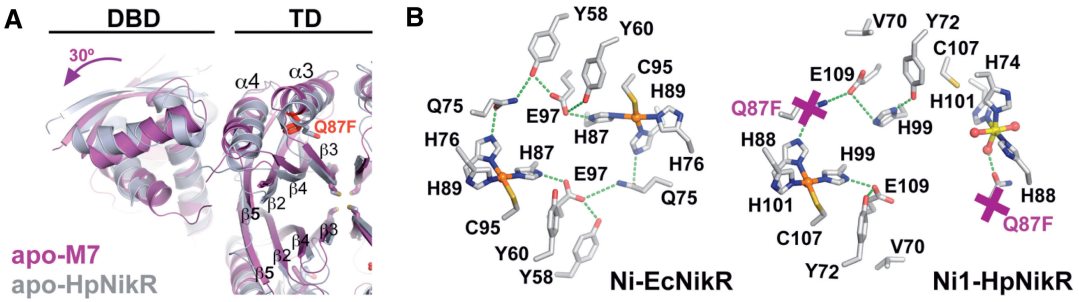

Figure 8. Apo-M7 structure suggests a weakening of β3–β′3 interactions and the disruption of the hydrogen bond network. **(A)** Detailed comparison of apo-HpNikR (grey) with apo-M7 (violet) in a view perpendicular to the 2-fold crystallographic axis showing the modifications induced by Q87F mutation (F87 side chain is indicated in red) at the tetramerization interface. The M7 structure was superimposed onto apo-HpNikR TD [r.m.s deviation of 1.76 Å (308 Cα)]. Accommodation of the F87 residue is accompanied by the displacement of α3 and α4 helices and the unzipping of β3–β′3 interactions at each side of the TD. These modifications unlock the TD interface and are echoed to the DBDs that adopt a modified closed *trans*-conformation. **(B)**. Detailed comparison of the conserved hydrogen bond network linking two nickel ions at the HA sites within each ACT-like pair observed in Ni-EcNikR (pdb code 2HZV) and Ni1-HpNikR structures.

an incomplete octahedral geometry in comparison with the Ni1-HpNikR structure.

Thus, Ni-M5 structure confirms that H74 and H75 are dispensable for nickel incorporation to HA sites. As expected, mutation of H74 and H75 suppressed the X site and destabilized the I site. Interestingly, a salt bridge is formed between D85 and R77 in the apo- and Ni-M5 (Figure 7B) as in apo-HpNikR structure. This D85–R77 interaction was not observed in Ni1–HpNikR, when Ni(II) is bound at the external X sites, suggesting that the secondary X sites might play a role in modifying R77 conformation.

M7 (Q87F) crystal structure displayed a modified *trans*-conformation and TD compared with apo-HpNikR structure (Figure 8A). In the M7 crystal structure, the adjustment of the F87 side chain within the hydrophobic core formed between β3 and β4 strands and α3 and α4 helices results in the displacement of α3 helices away from the interface at both sides of the TD. Hence, the rearrangement of α3 opens the TD interface and modifies the interactions between β3 strands that are found much more distant in M7 structure than in HpNikR structure (Figure 8). When M7 crystals were soaked in nickel solutions, no structure could be obtained with HA sites. When Ni(II) are bound to HA sites, an important hydrogen bound network is formed between neighbouring residues, including Q87 (Figure 8B). This network is conserved in all NikR structures and considerably stabilizes the coordination of nickel ions (15). Therefore, the main effect of Q87 mutation is the disruption of the hydrogen bond network. M7 mutant showed a considerably reduced affinity for DNA and also less stable HA site in the nickel-binding study. Together with the crystal structure of M7, these results suggest that the hydrogen bond network plays a crucial role in securing Ni(II) binding and thus in positioning HpNikR in a conformation suitable for DNA binding.

Finally, to investigate in detail the role of β3–β3 interactions, the structure of the M6 (C96S) mutant was also determined. C96 is unique to HpNikR and was found to have a pivotal role in the interactions between β3 strands (14). The TD from NikRs can be described as two pairs of ACT domains with Ni(II) binding between the ACTs (Figure 1) (42). ACT domains are regulatory modules that bind typically a small molecule to trigger conformational change for regulatory purpose (43). The M6 structure shows how a modification of the β3–β3 interactions, mediated by each ACT dimer, impacts on the positioning of the DBDs (Supplementary Figure S5, Table S2). C96 is thus instrumental for coupling the arrangement of the two ACT-like dimers upon nickel incorporation at HA sites and this could explain the slow kinetics of metal binding observed for this mutant.

DISCUSSION

In this study, we report a comprehensive analysis of the molecular properties of HpNikR and HpNikR mutants. Metal- and DNA-binding properties of purified mutant HpNikR proteins were investigated and their structures were determined by X-ray crystallography. In addition, SAXS experiments were performed to evaluate the conformation changes triggered by nickel incorporation in the protein and to gain insights into the activation mechanism of HpNikR. The evidences we assemble significantly improve our understanding of HpNikR activation and suggest a model for its activation that remarkably fits with the HpNikR properties described in the literature.

Structural basis of nickel sensing by the HA sites

We conclude that the HA sites are necessary but not sufficient to generate the active conformation of HpNikR. Together with our previous *in vivo* mutagenesis, the biochemical and structural analyses support that the hydrogen bond network bridging two HA sites plays a crucial role in the nickel-sensing mechanism. The hydrogen bond network prevents nickel dissociation from the HA sites and is necessary for the DNA binding.

Our data also clarify the role of the HA sites on HpNikR conformation. We show here that the protein adopts a defined conformation in solution and that nickel entry at the HA site does not generate large conformational changes of the DBDs. These findings contrast with the model proposed for EcNikR. The conformation observed is similar to the *cis*-conformation, i.e.

the one observed in the EcNikR/DNA complex. EcNikR was proposed to oscillate between open and closed *cis*- and *trans*-conformations both in its apo- and Ni(II) activated forms (16). EcNikR would then adopt a *cis*-conformation (17) only after contact with its DNA target possibly secured by potassium binding at the LA sites (17,27,44). Our work provides evidence that, in the case of HpNikR, the DBDs are not very flexible and might only require small rearrangements to accommodate DNA binding, which could explain the absence of requirement for LA sites (14,30). Differences of behaviour between EcNikR and HpNikR in solution were already described in the thermal denaturation studies. HpNikR showed no structural stabilization by Ni(II) binding (19) in contrast with EcNikR (22).

Role of the external site in HpNikR function

The importance of secondary external (X) sites in HpNikR activation has also been dissected. The X sites are not required for Ni(II) incorporation to the HA but affect DNA-binding activity. We show that the occupancy of the X site triggers small conformation changes in the β2–α3 loop containing Q76 and R77. The equivalent residues of EcNikR (K64 and R65) were found to interact directly with the DNA backbone in the EcNikR/DNA complex (17) and in HpNikR R77 could possibly interact with the DNA backbone as modelled in Figure 9. The mutagenesis study we described shows that Q76 and R77 are determinants for DNA binding in HpNikR. Interestingly, R77 forms a salt bridge with D85 from the adjacent subunit in the apo-HpNikR structure suggesting that the binding of Ni(II) to the secondary X site destabilizes the salt bridge and releases R77. This suggests a new regulation mechanism in which the metallation of the external X site could trigger the interaction of R77 with DNA. This mechanism might also explain the binding of HpNikR to p_{ureA} in the absence of nickel recently observed at low pH (29). Indeed, at low pH, the salt bridge between D85 and R77 could be disrupted and, together with a HpNikR *cis*-conformation we described, may be sufficient to generate an active form of HpNikR.

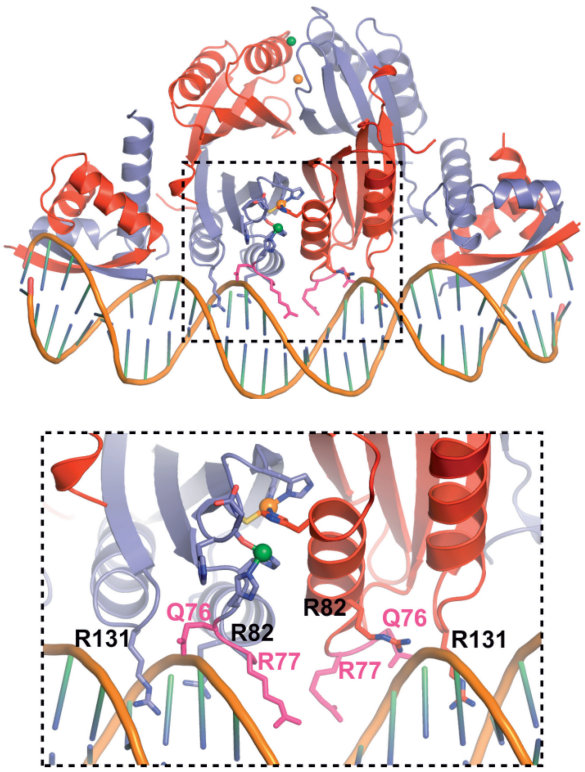

Figure 9. X sites tune the DNA-binding properties of HpNikR through the stabilization of β2–α3 loop and R77 availability. **(Top)** Theoretical model of the Ni–HpNikR–DNA ternary complex based on Ni–EcNikR–DNA complex. **(Bottom)** Detailed view of a model of HpNikR in closed *cis*-conformation bound to DNA, displayed in ribbon representation with chains B/D and A/C of HpNikR coloured in red and blue, respectively. Nickel ions bound to HA and X sites are indicated as sphere and coloured in orange and green, respectively. Amino acids from the TD involved DNA contacts are shown as balls and stick and coloured by atom type (carbon depending on the chain, green; oxygen, red and nitrogen, blue). Residues mutated in the M10 mutant are coloured in pink.

Metal requirement for HpNikR

HpNikR regulates the transcription of a large number of genes that have different promoter regions. To explain how HpNikR modulates the transcription of these genes, a two-tiered mode of recognition for the different HpNikR promoter regions was proposed, based on DNA promoter sequences and their affinity for HpNikR (11). One set of genes (*ureA*, *nixA*, *fecA3* and *frpb4*) has HA promoters and another one displays LA promoters for HpNikR (*fur*, *exbB* and *nikR*) (11). We show here that HA operators could be bound in Ni(II) only conditions by HpNikR, while the second category required Mn(II) for efficient binding. Since the geometry and ligands of the X site are compatible with binding of Mn(II) ions, we therefore propose that Mn(II) binding at X could be responsible for the regulation of the genes with 'LA' promoter by disrupting the R77–D85 salt bridge and increase HpNikR/DNA affinity.

Towards a model for HpNikR regulation of *H. pylori* metal homeostasis

In the light of the results presented here, we can propose a model for HpNikR regulation based on this work and on previous findings (Figure 10). This model could explain how HpNikR modulates the expression of various genes as a function of the metal ions. This regulation mechanism, specific to *H. pylori*, may allow for a gradual response to large variability in metal concentrations encountered in the gastric environment as a function of diet and/or of metal exposure (45). The mechanism also reflects possible differences of nickel regulation requirements between *H. pylori* and *E. coli*. HpNikR regulates the import of nickel only when excess is reached, but can also increase the expression of urease and other nickel-utilizing proteins. The evolution of the secondary external X site in HpNikR, located in the vicinity of DNA-binding residues, might provide an additional metal-based regulation mechanism. This mechanism might not be conserved in EcNikR and would explain a

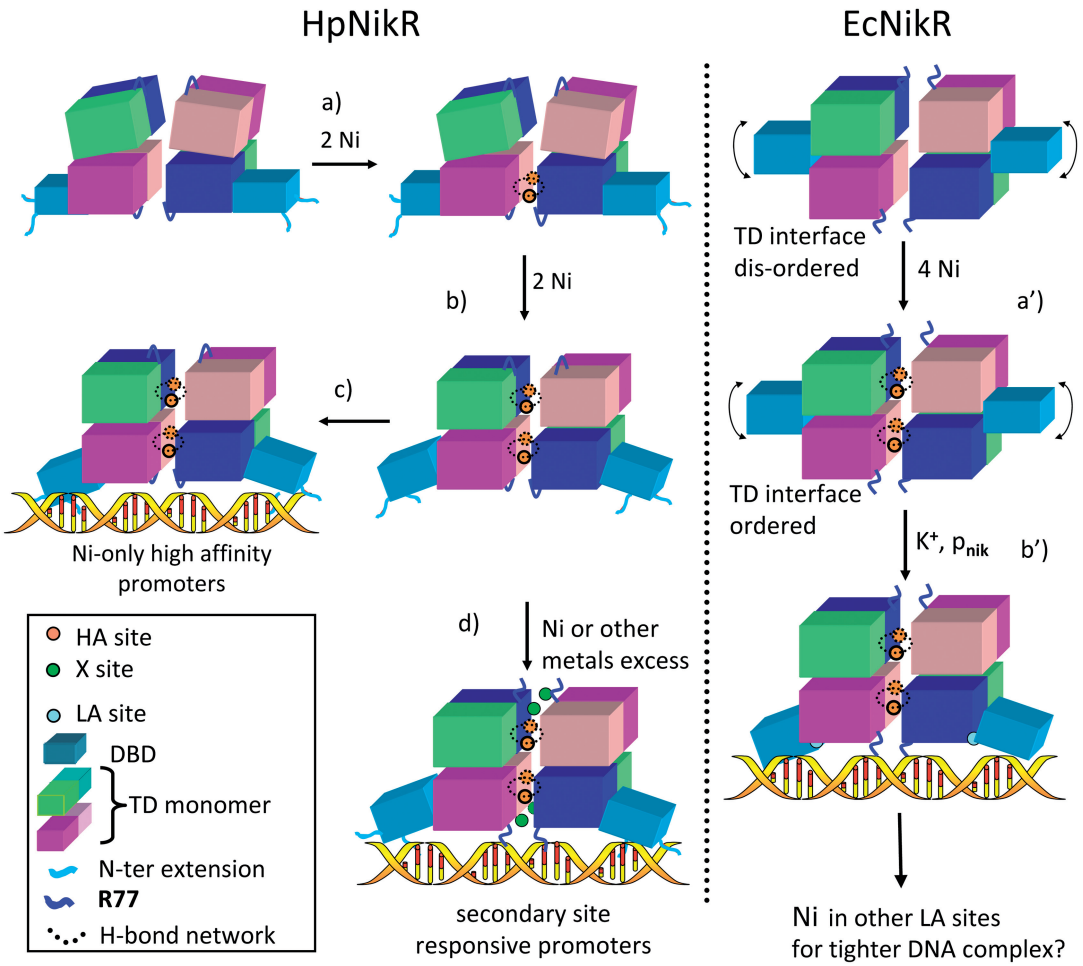

Figure 10. Schematic representation of the regulation mechanisms of the NikR proteins in *H. pylori* (left) and *E. coli* (right). We hypothesize that EcNikR and HpNikR use similar allosteric regulation of their ACT domains by nickel entry at the HA sites (**a, b and a′**). These changes are secured by the formation of the hydrogen bound network. In both proteins, this H-bond network is essential to the activation for DNA binding. Although this mechanism is likely to be common for NikR proteins, the conformation of all NikR proteins may not be the same in solution in apo form. This activation step would be sufficient for HpNikR to bind to high-affinity promoter regions (**c**). In a second step, species-specific mechanisms exist that are adapted to the nickel requirement by each organism. For HpNikR, the X site plays a role in modifying the position of DNA-interacting residues (such as Q76 and R77) from the β2–α3 loops (**d**). In EcNikR, this site seems unnecessary since these residues can readily interact with DNA without nickel-induced structural changes (17). Instead, EcNikR final conformation seems to require the LA site located between the TDs and DBDs that can bind potassium ion and lock the DBDs in a closed *cis*-conformation (**b′**). HpNikR might be completed by its unique N-terminal extension of nine amino acids required for specific DNA binding (28). This N-terminal extension has recently been shown to be involved in the pH-responsive DNA-binding activity of HpNikR (29).

stringent and direct repression of nickel import based only on the HA sites. However, Wang *et al.* (44) proposed a mechanism with a supplementary step for EcNikR regulation where the DNA-bound Ni–K–EcNikR complex is further strengthened by Ni(II) binding to other LA sites, hitherto location unknown, resulting in a significantly tighter DNA complex that completely arrests transcription. Thus, the question of the presence of additional sites in EcNikR playing a role similar to the X sites presented here for HpNikR remains open.

SUPPLEMENTARY DATA

Supplementary Data are available at NAR Online.

ACKNOWLEDGEMENTS

We thank Ulrike Kapp for her help for the crystallization assays and Catherine M. Delay and Sylvie Aubert for their help in the *in vivo* studies.

FUNDING

The French National Research Agency (ANR-07-BLAN-0083) with funding for the post-doctoral stays of C.B, C.D and C.M. Funding for open access charge: Commissariat à l'Energie Atomique (CEA).

Conflict of interest statement. None declared.

REFERENCES

1. Waldron,K.J. and Robinson,N.J. (2009) How do bacterial cells ensure that metalloproteins get the correct metal? *Nat. Rev. Microbiol.*, **7**, 25–35.
2. Dosanjh,N.S. and Michel,S.L. (2006) Microbial nickel metalloregulation: NikRs for nickel ions. *Curr. Opin. Chem. Biol.*, **10**, 123–130.
3. De Pina,K., Desjardin,V., Mandrand-Berthelot,M.A., Giordano,G. and Wu,L.F. (1999) Isolation and characterization of the nikR gene encoding a nickel-responsive regulator in *Escherichia coli*. *J. Bacteriol.*, **181**, 670–674.
4. Clyne,M., Dolan,B. and Reeves,E.P. (2007) Bacterial factors that mediate colonization of the stomach and virulence of *Helicobacter pylori*. *FEMS Microbiol. Lett.*, **268**, 135–143.
5. de Reuse,H. and Bereswill,S. (2007) Ten years after the first *Helicobacter pylori* genome: comparative and functional genomics provide new insights in the variability and adaptability of a persistent pathogen. *FEMS Immunol. Med. Microbiol.*, **50**, 165–176.
6. van Vliet,A.H., Poppelaars,S.W., Davies,B.J., Stoof,J., Bereswill,S., Kist,M., Penn,C.W., Kuipers,E.J. and Kusters,J.G. (2002) NikR mediates nickel-responsive transcriptional induction of urease expression in *Helicobacter pylori*. *Infect. Immun.*, **70**, 2846–2852.
7. Contreras,M., Thiberge,J.M., Mandrand-Berthelot,M.A. and Labigne,A. (2003) Characterization of the roles of NikR, a nickel-responsive pleiotropic autoregulator of *Helicobacter pylori*. *Mol. Microbiol.*, **49**, 947–963.
8. Ernst,F.D., Kuipers,E.J., Heijens,A., Sarwari,R., Stoof,J., Penn,C.W., Kusters,J.G. and van Vliet,A.H. (2005) The nickel-responsive regulator NikR controls activation and repression of gene transcription in *Helicobacter pylori*. *Infect. Immun.*, **73**, 7252–7258.
9. van Vliet,A.H., Ernst,F.D. and Kusters,J.G. (2004) NikR-mediated regulation of *Helicobacter pylori* acid adaptation. *Trends Microbiol.*, **12**, 489–494.
10. Delany,I., Ieva,R., Soragni,A., Hilleringmann,M., Rappuoli,R. and Scarlato,V. (2005) In vitro analysis of protein-operator interactions of the NikR and fur metal-responsive regulators of coregulated genes in *Helicobacter pylori*. *J. Bacteriol.*, **187**, 7703–7715.
11. Dosanjh,N.S., West,A.L. and Michel,S.L.J. (2009) *Helicobacter pylori* NikR's interaction with DNA: a two-tiered mode of recognition. *Biochemistry*, **48**, 527–536.
12. Ernst,F.D., Stoof,J., Horrevoets,W.M., Kuipers,E.J., Kusters,J.G. and van Vliet,A.H. (2006) NikR mediates nickel-responsive transcriptional repression of the *Helicobacter pylori* outer membrane proteins FecA3 (HP1400) and FrpB4 (HP1512). *Infect. Immun.*, **74**, 6821–6828.
13. Zambelli,B., Danielli,A., Romagnoli,S., Neyroz,P., Ciurli,S. and Scarlato,V. (2008) High-affinity Ni2+ binding selectively promotes binding of *Helicobacter pylori* NikR to its target urease promoter. *J. Mol. Biol.*, **383**, 1129–1143.
14. Dian,C., Schauer,K., Kapp,U., McSweeney,S.M., Labigne,A. and Terradot,L. (2006) Structural basis of the nickel response in *Helicobacter pylori*: crystal structures of HpNikR in Apo and nickel-bound states. *J. Mol. Biol.*, **361**, 715–730.
15. Schreiter,E.R., Sintchak,M.D., Guo,Y., Chivers,P.T., Sauer,R.T. and Drennan,C.L. (2003) Crystal structure of the nickel-responsive transcription factor NikR. *Nat. Struct. Biol.*, **10**, 794–799.
16. Chivers,P.T. and Tahirov,T.H. (2005) Structure of *Pyrococcus horikoshii* NikR: nickel sensing and implications for the regulation of DNA recognition. *J. Mol. Biol.*, **348**, 597–607.
17. Schreiter,E.R., Wang,S.C., Zamble,D.B. and Drennan,C.L. (2006) NikR-operator complex structure and the mechanism of repressor activation by metal ions. *Proc. Natl Acad. Sci. USA*, **103**, 13676–13681.
18. Abraham,L.O., Li,Y. and Zamble,D.B. (2006) The metal- and DNA-binding activities of *Helicobacter pylori* NikR. *J. Inorg. Biochem.*, **100**, 1005–1014.
19. Dosanjh,N.S., Hammerbacher,N.A. and Michel,S.L. (2007) Characterization of the *Helicobacter pylori* NikR-P(ureA) DNA interaction: metal ion requirements and sequence specificity. *Biochemistry*, **46**, 2520–2529.
20. Chivers,P.T. and Sauer,R.T. (2000) Regulation of high affinity nickel uptake in bacteria. Ni2+-Dependent interaction of NikR with wild-type and mutant operator sites. *J. Biol. Chem.*, **275**, 19735–19741.
21. Diederix,R.E., Fauquant,C., Rodrigue,A., Mandrand-Berthelot,M.A. and Michaud-Soret,I. (2008) Sub-micromolar affinity of *Escherichia coli* NikR for Ni(II). *Chem. Commun.*, 1813–1815.
22. Wang,S.C., Dias,A.V., Bloom,S.L. and Zamble,D.B. (2004) Selectivity of metal binding and metal-induced stability of *Escherichia coli* NikR. *Biochemistry*, **43**, 10018–10028.
23. Zambelli,B., Bellucci,M., Danielli,A., Scarlato,V. and Ciurli,S. (2007) The Ni2+ binding properties of *Helicobacter pylori* NikR. *Chem. Commun.*, 3649–3651.
24. Bloom,S.L. and Zamble,D.B. (2004) Metal-selective DNA-binding response of *Escherichia coli* NikR. *Biochemistry*, **43**, 10029–10038.
25. Chivers,P.T. and Sauer,R.T. (2002) NikR repressor: high-affinity nickel binding to the C-terminal domain regulates binding to operator DNA. *Chem. Biol.*, **9**, 1141–1148.
26. Phillips,C.M., Schreiter,E.R., Guo,Y., Wang,S.C., Zamble,D.B. and Drennan,C.L. (2008) Structural basis of the metal specificity for nickel regulatory protein NikR. *Biochemistry*, **47**, 1938–1946.
27. Phillips,C.M., Nerenberg,P.S., Drennan,C.L. and Stultz,C.M. (2009) Physical basis of metal-binding specificity in *Escherichia coli* NikR. *J. Am. Chem. Soc.*, **131**, 10220–10228.
28. Benanti,E.L. and Chivers,P.T. (2007) The N-terminal arm of the *Helicobacter pylori* Ni2+-dependent transcription factor NikR is required for specific DNA binding. *J. Biol. Chem.*, **282**, 20365–20375.
29. Li,Y. and Zamble,D. (2009) The pH-responsive DNA-binding activity of *Helicobacter pylori* NikR. *Biochemistry*, **48**, 2486–2496.
30. Danielli,A., Romagnoli,S., Roncarati,D., Costantino,L., Delany,I. and Scarlato,V. (2009) Growth phase and metal-dependent transcriptional regulation of the fecA genes in *Helicobacter pylori*. *J. Bacteriol.*, **191**, 3717–3725.
31. Horton,R.M., Ho,S.N., Pullen,J.K., Hunt,H.D., Cai,Z. and Pease,L.R. (1993) Gene splicing by overlap extension. *Methods Enzymol.*, **217**, 270–279.
32. Fauquant,C., Diederix,R.E., Rodrigue,A., Dian,C., Kapp,U., Terradot,L., Mandrand-Berthelot,M.A. and Michaud-Soret,I. (2006) pH dependent Ni(II) binding and aggregation of *Escherichia coli* and *Helicobacter pylori* NikR. *Biochimie*, **88**, 1693–1705.
33. Kabsch,W. (1993) Automatic processing of rotation diffraction data from crystals of initially unknown symmetry and cell constants. *J. Appl. Crystallogr.*, **26**, 795–800.
34. McCoy,A.J., Grosse-Kunstleve,R.W., Adams,P.D., Winn,M.D., Storoni,L.C. and Read,R.J. (2007) Phaser crystallographic software. *J. Appl. Crystallogr.*, **40**, 658–674.
35. Afonine,P.V., Grosse-Kunstleve,R.W. and Adams,P.D. (2005) A robust bulk-solvent correction and anisotropic scaling procedure. *Acta Crystallogr. D Biol. Crystallogr.*, **61**, 850–855.
36. Emsley,P. and Cowtan,K. (2004) Coot: model-building tools for molecular graphics. *Acta Crystallogr. D Biol. Crystallogr.*, **60**, 2126–2132.
37. CCP4. (1994) The CCP4 suite: programs for protein crystallography. *Acta Crystallogr. D Biol. Crystallogr.*, **50**, 760–763.
38. Vanet,A. and Labigne,A. (1998) Evidence for specific secretion rather than autolysis in the release of some *Helicobacter pylori* proteins. *Infect. Immun.*, **66**, 1023–1027.
39. Konarev,P.V., Volkov,V.V., Sokolova,A.V., Koch,M.H.J. and Svergun,D.I. (2003) PRIMUS: a Windows PC-based system for small-angle scattering data analysis. *J. Appl. Crystallogr.*, **36**, 1277–1282.
40. Svergun,D., Barberato,C. and Koch,M.H.J. (1995) CRYSOL – a program to evaluate X-ray solution scattering of biological macromolecules from atomic coordinates. *J. Appl. Crystallogr.*, **28**, 768–773.

41. Vitale,S., Fauquant,C., Lascoux,D., Schauer,K., Saint-Pierre,C. and Michaud-Soret,I. (2009) A ZnS4 structural zinc site in the *Helicobacter pylori* ferric uptake regulator. *Biochemistry*, **48**, 5582–5591.
42. Bradley,M.J., Chivers,P.T. and Baker,N.A. (2008) Molecular dynamics simulation of the *Escherichia coli* NikR protein: equilibrium conformational fluctuations reveal interdomain allosteric communication pathways. *J. Mol. Biol.*, **378**, 1155–1173.
43. Grant,G.A. (2006) The ACT domain: a small molecule binding domain and its role as a common regulatory element. *J. Biol. Chem.*, **281**, 33825–33829.
44. Wang,S.C., Dias,A.V. and Zamble,D.B. (2009) The "metallo-specific" response of proteins: a perspective based on the *Escherichia coli* transcriptional regulator NikR. *Dalton Trans.*, 2459–2466.
45. Sunderman,F.W. Jr (1993) Biological monitoring of nickel in humans. *Scand. J. Work Environ. Health*, **19(Suppl. 1)**, 34–38.